

REPORT DOCUMENTATION PAGE

DO NOT WRITE IN THESE SPACES BEFORE COMPLETING FORM

1. REPORT NUMBER	2. GOVT ACCESSION NO.	3. RECIPIENT'S CATALOG NUMBER
4. TITLE (and Subtitle) PARTICLE SIZE MEASUREMENTS IN SOLID PROPELLANT ROCKET EXHAUST PLUMES		5. TYPE OF REPORT & PERIOD COVERED FINAL REPORT 11 Jun 77 - 30 Jun 1978
6. AUTHOR(s) Kenneth E. Harwell / Project Director W. M. Farmer / Co-Principal Investigator <i>Michael</i>		7. CONTRACT OR GRANT NUMBER(s) N00174-77-C-0234
8. PERFORMING ORGANIZATION NAME AND ADDRESS The University of Tennessee Space Institute Tullahoma, TN 37388		9. PROGRAM ELEMENT, PROJECT, TASK AREA & WORK UNIT NUMBERS
10. CONTROLLING OFFICE NAME AND ADDRESS Naval Ordnance Station Attn: Code 1141 Indian Head, MD 20640		11. REPORT DATE 30 June 1978
12. MONITORING AGENCY NAME & ADDRESS (if different from Controlling Office) Naval Ordnance Station Attn: Dr. Charles B. Dale Code: 525A Indian Head, MD 20640		13. NUMBER OF PAGES 39 pages
14. DISTRIBUTION STATEMENT (of this Report) Approved for public release; distribution unlimited		15. SECURITY CLASS. (of this report) UNCLASSIFIED
16. DISTRIBUTION STATEMENT (of the abstract entered in Block 20, if different from Report)		17. DECLASSIFICATION/DOWNGRADING SCHEDULE

ADA 078556

LEVEL

DDC  
REPRODUCTION  
SEP 10 1979  
UNLIMITED

18. SUPPLEMENTARY NOTES

19. KEY WORDS (Continue on reverse side if necessary and identify by block number)

Rocket Exhaust Plumes  
Particle Size Measurements  
Laser Velocimetry

79 09 002

20. ABSTRACT (Continue on reverse side if necessary and identify by block number)

Particle sizing interferometer measurement of particle size distributions, velocity and number density in samples of rocket propellant exhaust is described. Signal visibility and scattered intensity for individual particles was measured for a nominal size range of 0.3 to 6 micrometers. Calibration tests of the instrument were obtained by firing small propellant samples into a 20-m<sup>3</sup> chamber and comparing the measured particle size distributions with those obtained from estimates using multiple wavelength transmissometers and a commercial optical particle counter. Particle sizing interferometer estimates of particle size distributions (OVER)

DDC FILE COPY

387010

20 ABSTRACT (cont.)

and number densities required the development of models which could account for sample space dependence on particle size and illuminating fringe contrast variation. Results obtained by using these models on particle size data from calibration and rocket motor test firings show the need for well-controlled insitu perturbati less particle size measuring techniques for hostile environments.

A

Accession For	
NTIS G&I	<input checked="" type="checkbox"/>
LES TAB	<input type="checkbox"/>
Un announced	<input type="checkbox"/>
Justification	
By	
Distribution/	
Availability Codes	
Dist	Avail and/or special
A	

**DISPOSITION INSTRUCTIONS**

**DESTROY THIS REPORT WHEN IT IS NO LONGER NEEDED. DO NOT RETURN IT TO THE ORIGINATOR.**

**DISCLAIMER**

**THE FINDINGS IN THIS REPORT ARE NOT TO BE CONSTRUED AS AN OFFICIAL DEPARTMENT OF THE ARMY POSITION UNLESS SO DESIGNATED BY OTHER AUTHORIZED DOCUMENTS.**

**TRADE NAMES**

**USE OF TRADE NAMES OR MANUFACTURERS IN THIS REPORT DOES NOT CONSTITUTE AN OFFICIAL INDORSEMENT OR APPROVAL OF THE USE OF SUCH COMMERCIAL HARDWARE OR SOFTWARE.**

Final Report

U.S. Navy Contract N00174-77-C-0234

PARTICLE SIZE MEASUREMENTS IN SOLID  
PROPELLANT ROCKET EXHAUST PLUMES

Kenneth E. Harwell, Project Director and  
W. Michael Farmer, Co-Principal Investigator  
The University of Tennessee Space Institute  
Tullahoma, Tennessee 37388

30 June 1978

Approved for public release; distribution unlimited

Prepared for  
U.S. Navy  
Naval Ordnance Station  
Indian Head, Maryland 20640

## ACKNOWLEDGEMENTS

The contract monitor for this program was Dr. Charles B. Dale of the U.S. Naval Ordnance Station, Indian Head, Maryland.

The support of Dr. Walt Wharton and L. B. Thorne of the U.S. Army Missile Research and Development Command in allowing UTSI to make PSI measurements in the U.S. Army Signature Characterization Facility at Redstone Arsenal is noted with appreciation.

The PSI measurements in the exhaust plume of a small rocket motor were conducted at the NAVSEA Allegany Ballistic Laboratory rocket static test facilities near Cumberland, Maryland. The assistance and support of ABL contractor, Hercules, Inc., enabled the test program to be conducted. The efforts of Mr. Don Sine, Mr. Tom Durney and Mr. Gene Moore were beneficial to the effort and are greatly appreciated.

The assistance of Mr. George Buckle, NAVSEA Low Signature Program Manager, NOS (Indian Head), in arranging the NAVSEA ABL test program is also gratefully acknowledged.

The authors acknowledge the assistance of Mr. James O. Hornkohl and Mr. Fred Schwartz who were responsible for the electronics systems and data acquisition.

## ABSTRACT

Particle sizing interferometer measurement of particle size distributions, velocity and number density in samples of rocket propellant exhaust is described. Signal visibility and scattered intensity for individual particles was measured for a nominal size range of 0.3 to 6 micrometers. Calibration tests of the instrument were obtained by firing small propellant samples into a 20-m<sup>3</sup> chamber and comparing the measured particle size distributions with those obtained from estimates using multiple wavelength transmissometers and a commercial optical particle counter. Particle sizing interferometer estimates of particle size distributions and number densities required the development of models which could account for sample space dependence on particle size and illuminating fringe contrast variation. Results obtained by using these models on particle size data from calibration and rocket motor test firings show the need for well-controlled insitu perturbationless particle size measuring techniques for hostile environments.

## NOMENCLATURE

$A_i$	cross-sectional area for sample space of the $i$ th particle size
$A_{mx}$	maximum observable cross-sectional area of sample space
$A_o$	cross-sectional area for sample space of a particle with diameter $D_o$
$b$	intercept of a linear least squares curve fit for X versus Y
$b_o$	$e^{-2}$ mean irradiance radius of geometric probe volume
$D$	spherical particle diameter
$dG/d\Omega$	differential scattering gain
$d\sigma/d\Omega$	differential scattering cross-section
$e$	electron charge
$f_i$	fraction of particles with diameter $D_i$
$g$	PMT dynode gain
$I_o$	irradiance incident on a particle
$I_s$	scattered radiant power collected by the receiver system
$i_s$	signal current at the output of a photomultiplier tube (PMT)
$m$	$Z \sin(\alpha/2)/b_o$
$N$	particle number density
$\dot{N}$	data acquisition rate
$N_{ci}$	numeric count for $i$ th particle size histogram increment
$P$	slope of a linear least squares curve fit for X versus Y

$q$	quantum efficiency of phototube
$\Delta t$	total sample time
$V_i$	velocity of $i$ th particle
$X$	$D/\delta$ , where $\delta$ is PSI fringe period
$Y$	square root of integrated mean value of signal magnitude
$Z$	sample space coordinate parallel to bisector between the illuminating beams
$\alpha$	angle between illuminating beams
$\bar{\tau}$	mean signal time period
$\psi_i$	system response weighting factor for $i$ th particle size histogram bin
$\phi(D)$	scattered signal phase dependent on particle scattering parameters
$\omega_D$	Doppler difference frequency
$\Omega$	solid angle subtended by the scattered light receiver

## 1.0 INTRODUCTION

A knowledge of particle size distributions in the primary and secondary smokes generated by solid rocket motor combustion processes is of fundamental importance for accurately modeling both the combustion process and subsequent smoke formation. Such models serve the two fold purpose of characterizing the optical signature of propellants and of predicting general propellant combustion properties from the knowledge of the propellant chemistry.

For all practical purposes it is impossible to sample mechanically real rocket exhausts during an actual firing. The environment is fluctuating too rapidly and a probe perturbs the flow. Optical techniques are therefore the only truly suitable means of measuring particle size. However, there are extreme conditions which must be overcome if particle size measurements are to be obtained with any optical instrument. One of the most significant problems in this regard is that associated with background light in the exhaust. This light results from radiant gas emission and the black body radiation of hot particles located in the exhaust. The difficulty in measuring such particles is further compounded by the facts that 1) they may have extremely high velocity (on the order of kilometers per second), 2) the number density may often be very high (at times exceeding  $10^7$ /cc) and 3) the particle chemistry is probably not known leading to large uncertainties in particle indices of refraction. Furthermore, the particles can be expected to be small (of the order of 1-10 micrometers or less) which precludes numerous photographic and holographic techniques which might be used otherwise. During the past year the Gas Diagnostics Research Division at The University of Tennessee Space

Institute has been involved in preliminary studies to determine the feasibility of applying a particle sizing interferometer (PSI) to the measurement of such particles. To this end both analytical feasibility studies and experimental research have been conducted to determine the magnitude of the problems which may be encountered in obtaining these kinds of particle size measurements.

As outlined in the statement of work for the research project, the original program plan was to validate the experimental technique by conducting a set of calibration tests in which particles of known size would be injected into the exhaust plume of a small rocket motor operating under cold flow conditions. Experimental data obtained using the particle sizing interferometer were to be compared with particle size data obtained using a cascade impactor or wire grid system. As originally outlined in the proposal, these cold-flow calibration tests were necessary prior to conducting particle size and concentration measurements in the exhaust plume of a small rocket motor.

Due to limited contract funds, which prevented all the proposed tasks to be funded, an alternate test plan was evolved in which PSI measurements were made of rocket exhaust particles obtained from the combustion of small samples of rocket propellant fired into a large 20-m<sup>3</sup> environmental chamber at Redstone Arsenal.<sup>1</sup> In addition to these PSI measurements, some preliminary "piggy-back" measurements were made of particles in the edge of a small rocket motor plume at the NAVSEA Allegany Ballistic Laboratory, Cumberland, Maryland.

The PSI measurements obtained as part of the effort under this contract are compared with particle size data obtained using a commercial optical counter and a multiple wavelength transmissometer.

The purpose of this report is to describe the results obtained as part of this contract effort, to discuss the comparison between experimental data obtained using the different experimental techniques, and to describe some of the features of the rocket plume measurements.

Since the theoretical basis for the particle sizing interferometer and the calibration procedure have been described previously,<sup>2</sup> only the specific optical and electronic system details required to understand the experimental results will be described in this report.

## 2.0 OPTICAL SYSTEM DESCRIPTION

Two slightly different forward scatter optical system geometries were used for these measurements. The first geometry, shown in Fig. 1, was used for the measurements in the mixing chamber at Redstone Arsenal. It is a forward scatter dual-scatter or differential Doppler system. The distinguishing feature about this system is the collection of forward scattered light with a variable focus receiver system which reflects the light back outside the mixing chamber where it is then relayed to a photomultiplier tube. The purpose for this particular geometry results from the fact that the chamber may be cooled to less than  $-30^{\circ}\text{C}$  or heated to greater than  $+30^{\circ}\text{C}$  and the relative humidity may be controlled between 20% and 100%. Furthermore, since the rocket propellants tested can be quite corrosive (particularly those which produce hydrogen chloride exhaust products) it was desirable to minimize environmental exposure. The laser used in this system is a Spectra Physics Model 124A which produces approximately 30 milliwatts of light power. The fringe period generated by the transmitting optics was typically set to about 6 microns. Because the lenses used in the transmitter portion of the system have relatively low F numbers ( $\sim 2-3$ ) with spherical aberration and astigmatism,

the sample space or probe volume had an elliptical cross-section.

The cross-section was approximately 50 interference fringes wide in a direction normal to the fringe planes and approximately 20 fringe periods wide in a direction parallel to the fringe planes. An adjustable slit was used in the receiver geometry immediately in front of the photomultiplier tube (EMI-9781R). It was set at a sufficient width to allow the return image of the geometric probe volume to pass with little or no diffraction. The photomultiplier tube housing was connected to a dual channel preamp which was used to transmit the signal to the visibility and signal time period processing electronics. The preamp separately amplified the mean and the Doppler components of the signals.

The second optical system, used in the rocket plume measurement, is shown in Fig. 2. Because there was no need to separate the transmitter and receiver system, a standard forward scatter optical system geometry was used. The laser, preamp, and electronics systems were identical to those in the first system. This system was mounted in a box for environmental protection during motor firings. The box was built of 3/4" plywood and painted black to minimize interference with transmissometer measurements which were made through the plume. The entire inner portion of the box was lined with foam rubber 2" thick. This was found to be more than sufficient both for temperature insulation (measurements were made at ABL at the end of the previous winter) and for protection from the shock waves present during motor ignition. A photograph of the test setup is shown in Fig. 3. Both optical systems were mounted on a 1.3-cm thick, 0.6 x 1.2-m aluminum base plate. The fringe period in the second system was set to be approximately 10 microns and the limiting aperture at the photomultiplier tube was set such that the depth of

field determined by the receiver lens aperture combination was approximately 1/4 that of the geometric probe volume.

### 3.0 ELECTRONIC SYSTEM DESCRIPTION

A block diagram of the electronic system used for processing the scattered light signal and for acquiring and manipulating the data is shown in Fig. 4. In this configuration the signal is divided into two portions; one portion enters the visibility processor and one portion enters the velocity processor and data acquisition system. The velocity processor provides signal logic tests for multiple particle signals, signal dropouts, acceptable aperiodicity and improper particle trajectory. These tests are used as the control logic for accepting or rejecting signals measured by the visibility processor. The lower portion of the figure shows the approach we have taken in obtaining a visibility measurement. One portion of the signal is integrated directly. This integral yields a mean value, or pedestal portion of the signal. The second portion is filtered to remove the pedestal, and then full wave rectified and integrated. This measurement yields a value which is proportional to the energy in the sinusoidal portion of the signal. In each leg of the visibility processor four multiplexed integrators are used in order to obtain a signal dynamic range of approximately  $1:10^4$  with three digit accuracy. After the integrations are complete the values for the AC (sinusoidal) and the DC (mean value) components of the signal are sent to a small microprocessor memory where they are recorded along with the signal time period measurement. The velocity processor can be programmed to perform signal time period averages over a large and small number of signal periods. This number can range between 2 and 256 on both the large and small averages. The acceptable aperiodicity in the signal is determined by the difference in the large and small number of cycles time averages. For brevity these averages are called long and

short counts. The acceptable aperiodicity is also programmable from 0.1 to 50%. The velocity processor has a so-called dropout detector which allows the processor to immediately recycle the instrument if particle trajectories or noise are such that the signal has an insufficient number of cycles to meet the criteria imposed upon the signal processor logic.

After a sufficient data set has been obtained (the number of measurements which can be entered into memory is also programmable), a set of prechosen software programs are used for data manipulation and computation. A summary of these programs is given in Appendix I. One program computes the statistics associated with particle velocity. The parameters computed are 1) mean particle velocity, 2) standard deviation of the velocity distribution expressed as a percent of mean velocity, and 3) the Kurtosis of the velocity distribution. The particle size program includes histograms of particle size based on a spherical particle visibility function which is permanently in memory and the correlation of two measurements of particle size. The measurements are determined from the visibility and from the scattered intensity magnitude of the signal. Finally the entire data set which is in memory (the signal time period, the magnitude of the signal mean value and the magnitude of the AC integral) can be displayed along with the equivalent particle sizes from signal visibility and relative scattered magnitude. A typical sample of the microprocessor output is given in Table I.

The program which is used to correlate particle size as determined from scattered intensity and that which is determined from a visibility measurement has produced some interesting results. The logic which enters into it is as follows. The magnitude of the scattered intensity is given in Equation 1:

$$I_s = I_o \int_{\Omega} \frac{d\sigma}{d\Omega} d\Omega \quad (a) \quad (1)$$

$$\frac{d\sigma}{d\Omega} = \frac{\pi D^2}{4} \frac{dG}{d\Omega} \quad (b)$$

For a dual beam PSI system  $dG/d\Omega$  can be written in the form

$$\frac{dG}{d\Omega} = \left. \frac{dG}{d\Omega} \right|_1 + \left. \frac{dG}{d\Omega} \right|_2 + \left. \frac{dF(G_1, G_2)}{d\Omega} \right|_{12} \cos(\omega_o t + \phi(D)) \quad (2)$$

where the subscripts denote the scatterers gains for the respective beams. The signal current generated by the scattering process can be written as

$$i = q e g P_s \quad (3)$$

The mean value of the scattered light signal with respect to time will be linearly proportional to  $\left. \frac{dG}{d\Omega} \right|_1 + \left. \frac{dG}{d\Omega} \right|_2$  since the cosine term averages to zero. Hence, the signal current measured by the pedestal integrators is proportional to the square of the particle diameter multiplied by some factor dependent on the sum of the individual scatter gains, and the incident light flux. This factor will be a variable depending upon the trajectory of the particle and the sensitivity of the scatter gain as a function of particle size. Classical diffraction theory shows that when the observation aperture is sufficient to collect a large portion of the forward scattered lobe from the particle, then the scatter gain will be approximately constant, and that in the region where it is not constant it may be roughly approximated as a linear function of the particle diameter.<sup>3</sup> If we assume that the scatter gain is independent of particle diameter then the square root of the signal

current should be proportional to particle diameter. Experimentally, this factor will be a variable which depends upon the trajectory of the particle through the sample space or equivalently upon the incident light flux. The variability can be made small by suitable apertures in the receiver optics. In the software program under consideration, the square root of the pedestal magnitude is computed and is assumed to be proportional to particle diameter to within some system calibration constant. The ratio of particle diameter to fringe period as determined from the spherical particle visibility function is also computed and linear least squares curve fit of these parameters is made of the form:

$$Y = pX + b \tag{4}$$

Hence, given a Y value from the scattered signal magnitude, an equivalent  $D/\delta$  value can be computed. A simple model will illustrate how this is achieved. For particles and an optical system where the scatter gain can be assumed to be nearly independent of particle diameter it can be shown that the cross-sectional area  $A_i$  of the sample space for some particle diameter  $D_i$  is given by

$$A_i = A_o D_i / D_o \tag{5}$$

and  $A_o/D_o$  is a calibration factor dependent upon the scattering efficiency of the calibration particle, the optical system geometry, and the signal processor sensitivity and logic constraints.<sup>4</sup>  $A_i$  enters into the response function of the PSI in the following manner. The number density for a particular particle size can be written as

$$N_i = \dot{N} f_i / V_i A_i \tag{6}$$

where  $V_i$  is the particle velocity,  $\dot{N}$  is the rate at which  $D_i$  is measured and  $f_i$  is the fraction of particles with diameter  $D_i$ . The factor  $V_i A_i$  when properly normalized yields a set of weighting factors for each of the particle size increments which when multiplied by the number of measurements obtained for some particle size yields the effective number of particles measured in a unit volume. Because of the constraints imposed on acceptable signals by the signal processor, the  $A_i$  values cannot become infinitesimally small as  $D_i$  approaches zero. The long count requirement for the particle trajectory implies a minimum acceptable cross-section area. Hence, if a plot is made of the weighting factors as a function of particle size for a particular instrument, it will appear to become discontinuously constant at some particular size. In this simple model we assume that the sample space is identical to the geometrical probe volume defined by the  $e^{-2}$  mean intensity contour. Using this assumption the cross-sectional area of the sample space is estimated as the cross-sectional area of an oblate ellipsoid. The long count programmed in the signal processor is then taken to be the minimum acceptable trajectory which passes through the sample space cross-sectional area. The equations describing the ellipsoid are solved to estimate the minimum cross-sectional area specified by a particle trajectory corresponding to a long count. The ratio between this minimal area and the maximal area determined by the  $e^{-2}$  contour is assumed to be the allowable range of weights which may be assigned to the particle size distribution.

Since it is assumed that the receiver system is set up to view the entire  $e^{-2}$  contour probe volume the fact that the visibility of the interference fringes illuminating the particle is a function of where the particle passes through the probe volume must also be taken into account in the system response function.<sup>5</sup> The signal processor is constructed such that a proper multiplier

is supplied in the visibility computation for all particle trajectories passing through the geometric center of the probe volume. Column 2 in Table II shows that a multiplier for  $z = 0$  (i.e., for trajectories passing through the geometric center of the probe volume) will be too small for trajectories not passing through the center because the visibility is reduced. It is reasonable to conclude from Table II that the bins in a PSI particle size histogram which correspond to small to intermediate values of the visibility will contain an erroneously high particle count. The high count will result from measurements of particles which should have been counted in a smaller size bin but produced signals with reduced visibility due to trajectories which do not pass through the geometric center of the probe volume. To correct for these erroneous counts a set of weighting factors was determined which enter into the system response function along with the volumetric normalization values. These factors for various values for  $m$  are shown in Table II.

A rough estimate of the particle number density using PSI measurements may be obtained by determining  $A_{mx}$ , the maximum sample cross-sectional area observed during the particle sizing measurements.  $A_{mx}$  is experimentally determined by observing the output of the zero crossing detector in the velocity processor and thereby measuring the maximum number of cycles in the signal during any one particular experiment. The absolute number density,  $N$ , can then be written as

$$N = \frac{\bar{\tau} \alpha}{A_{mx} \delta \Delta t} \sum_{i=1}^{2l} N_{ci} \psi_i' \quad (7)$$

It was found that the value of  $A_{mx}$  for the experiments reported in this paper was approximately  $1.7 \cdot 10^{-2} \text{mm}^2$ .

#### 4.0 EXPERIMENTAL RESULTS

The optical system shown in Fig. 1 was used in the mixing chamber tests. Calibration tests were performed in the mixing chamber using urea-formaldehyde resin particles which are spherical, translucent, and remarkably monodisperse for a non-liquid particle. The PSI system was focused approximately 15" inside the mixing chamber and approximately 30" from the floor of the chamber. The optical commercial optical counter sampling tube was located near the top of the chamber. The urea-formaldehyde was injected into the chamber and maintained in suspension by a set of small electric fans which maintained a counterclockwise circulatory pattern near the top of the chamber. Figure 5 shows a set of histograms obtained with the PSI for the urea-formaldehyde measurements. The histograms from the PSI are plotted as solid lines while those obtained with the commercial optical counter are plotted as dashed lines. There exists obvious discrepancies between the two sets of data. The commercial counter consistently counts a large number of particles less than 1 micron. The mode sizes for the two distributions in the urea-formaldehyde range roughly agree. It is interesting to observe the time history dependent size distribution as observed with the PSI system. We note that before particle injection the background particle sizes were predominately less than about 1.5 microns and the particle number density is surprisingly low (see Fig. 6). The PSI sample space is located well below the fan circulation plane and air movement is of relatively low volume in this area. The commercial counter on the otherhand has its sampling tube located near the top of the chamber where there is considerable air circulation and it mechanically withdraws an air sample at

a fairly high rate. We notice that after the urea-formaldehyde particles are injected the background particle count immediately becomes over-shadowed by the urea-formaldehyde particles until approximately one minute after dust injection, the background count is virtually non-existent in the particle size histogram. We note also that the size distribution parameters remain roughly constant throughout the sample time of the experiment although there are minor changes in the standard deviation of the measurements. This variation is to be expected due to the different number of particles which were sampled during that time. Figure 6 plots the number density of the urea-formaldehyde particles as estimated from the PSI measurements using some of the simple models previously described. A least squares linear logarithmic analysis was found to fit the data. It should be expected that the particles will settle out of the chamber and be driven to the walls by the circulation fans. Thus, the number density will decrease with time and theoretical predictions suggest that the decrease should be exponential.<sup>6</sup> It is interesting to note that near the beginning of the set of measurements, the optical counter and the PSI were in close agreement on the particle number density and that as time increased the number density observed with the PSI system fell off at a higher rate than that obtained with the commercial counter which sampled the aerosol at a constant rate. This data thus hints at the possibility of data biasing errors in terms of number density measurements due to the location of mechanical sampling probes and in mechanically withdrawing a sample at a constant rate.

After the urea-formaldehyde tests, the PSI system was applied to measurement of rocket exhaust particles obtained from small propellant samples fired into the mixing chamber. For the measurements reported here the mixing chamber

was kept at a temperature of approximately 20.2°C and a relative humidity of 20%. Figure 7 shows an example of the estimated number density as a function of time for these measurements. The number density as determined by the commercial optical counter is plotted in the same figure and again shows that while initially the particle number densities as determined by the two instruments are in reasonable agreement, the optical counter which is mechanically withdrawing an aerosol sample yields a much slower particle fallout rate than that determined by the PSI. Figure 8a shows the size distribution approximately 1.33 minutes after propellant ignition and represents approximately 440 particle measurements. It reveals a distinctly bimodal size distribution with one mode occurring at less than 0.5 micrometers. We observe that there is good agreement in the commercial optical counter and PSI measurements for the values of the small mode size and near the edge of the large mode size during the time interval between 1.33 and 3.95 minutes (Fig. 8b). The small size mode peaked at about 72% probability of occurrence and then decreased to zero. The large mode on the otherhand fell to about 4% and then rose to a value of about 15-20%. The small size mode continued to decrease and the large size mode increased until at approximately 8.6 minutes (Fig. 8c) the small size mode had virtually disappeared leaving only the large size mode distribution which was close to the background size distribution before ignition.

Figures 8a-c were chosen to make the PSI measurements correspond as closely in data recording time with the commercial optical counter as possible and still be representative of the overall time history of the measurements. The PSI histograms are also plotted in terms of 0.55 micrometer intervals in order to more closely correspond to the commercial counter intervals for the smaller sizes although the data was acquired in 0.275 micrometer intervals.

It is difficult to compare directly the results between the PSI and commercial optical counter because the commercial counter sample tubing is outside the test chamber. The aerosol sample withdrawn from the chamber will be cooled when the chamber is above ambient temperature (as was this case) and warmed when it is below. Furthermore, the commercial counter size increments were much coarser than those of the PSI and because the index-of-refraction of the particles is not certain, its response function is suspect. Finally, the commercial counter samples approximately 200 times more volume per unit time than the PSI.

There are some interesting discrepancies in the two sets of measurements. The commercial counter does not reflect the bimodal distribution until very near the end of the test sequence. Its data suggests the initially the predominant mode size is less than 0.5 micrometers and that its resulting probability density is in close agreement with the PSI. It also shows a significant size fraction in the size range of 0.5 to 1 micrometers which the PSI does not and it shows the particle number density decreases at a slower rate than that of the PSI. In attempting to resolve these discrepancies it might be argued that the apparent bimodal distribution observed by the PSI is in reality due to a decrease in particle size resolution predicted by other workers who have used different visibility functions from those used here.<sup>7-9</sup> Their work suggests that the smallest resolvable particle size with the signal processor used in this work would be of the order of 1.6 micrometers.

Figure 9 compares the size distributions estimated using appropriate visibility functions taken from Refs. 5 and 7. The visibility function chosen from Ref. 7 assumes a particle index-of-refraction of 1.5 with a zero absorption index. For the experiment, the fringe period was approximately 6.6- $\mu\text{m}$  and receiver F number was 4.8. The theoretical calculation from Ref. 7

was for a fringe period of  $6.3\text{-}\mu\text{m}$  and a receiver F number of 5. Figure 9 shows that the visibility function from Ref. 7 does not adequately reconcile the differences in the data obtained with the PSI and the commercial counter. This visibility function shows modal sizes existing which are well beyond any estimated by the visibility function in Ref. 5 or the commercial counter. Furthermore, it also shows a small probability density where the commercial counter shows it is large. Thus, the differences in the size distributions measured by the PSI and commercial counter do not seem to stem from an uncertain visibility function. Numerous Hueristic arguments may be put forth to explain these discrepancies. For example, the different locations of the sample spaces for the two instruments, the fact that the commercial optical counter is calibrated in terms of latex spheres and hence the particle sizes determined by the optical counter are equivalent latex sphere sizes could all contribute to the discrepancies in the measurements. If the particles are irregularly shaped then the visibility function applied to the size determination will obviously be erroneous or can be interpreted as representing some kind of average size for the particle shape. A final and probably most significant factor could be large errors in the size distribution weighting factors which are used.

When the results from the PSI or the commercial counter are compared to those of the multiwavelength transmissometer there is considerable disagreement. Typical transmission values for visible wavelengths were between 60 and 80%. If it is assumed that all particles measured by the optical counter and the PSI are about 3 micrometers in diameter (the case for minimum transmission), then the estimated transmission would be greater than 93%. The difference between the measured transmission and that predicted from single particle counter measurements may be attributed to at least 2 factors. First, transmission

estimates based on size distributions obtained with optical counter measurements have not accounted for the absorption cross-section of the particles which is an unknown factor for all three sets of measurements. If the absorption cross-section of the measured particles is significant then it follows that

- 1) the commercial counter would become less sensitive (its response function decreases) for all particle sizes greater than 0.5 micrometers,<sup>10</sup>
- 2) then if the PSI is resolution limited as one theory suggests, the large mode size measured by the PSI would shift from about 2.9 micrometers to about 4.3 micrometers and
- 3) the optical counter would show fewer measurements of particle size larger than about 5 micrometers.

In view of the evidence a reasonable conclusion would seem to be that the absorption cross-section for the particles is large and that the PSI is not resolution limited for sizes less than 1.5 micrometers. A large absorption cross-section suggests particles which have a high metallic content which is consistent with sampling done for chemical analysis of the exhaust products. A second possible discrepancy may result from high number densities (for particles less than 0.3 micrometers) which probably cannot be detected by the PSI or commercial optical counter but which can yield significantly lower transmissivities. These particles can result from condensation nuclei which may grow or decay according to a thermodynamic characteristic of the sample chamber (see Ref. 11). However, if the parameters for a log-normal size distribution are estimated from the multiple wavelength transmissometer measurements, the number densities which could be measured by the individual particle instruments still do not agree with those predicted by the distribution function. Furthermore, for the number densities which are estimated ( $10^5$ /cc for a diameter of about 0.04 micrometers) the signals generated by the PSI would probably show an incoherent scattered light background resulting from multiple particles simultaneously in the sample space.

Real time observation of the PMT current with an oscilloscope showed no such background.

PSI measurements made in the edge of a small rocket plume were made using the optical system shown in Fig. 2. The size range covered by the PSI was roughly 0.5 to 10 micrometers. The sample space of the PSI system was focused at the edge of the plume such that the particle velocity measured was only 3 or 4 m/sec. Several different solid propellant formulations were examined. Each propellant was found to have a unique particle size histogram. The particle modal sizes ranged between 0.5 and 10 microns. During operation only approximately 0.3 seconds of the total rocket motor firing could be examined because of the limited data memory possible with the current system (900 measurements). These data were obtained as part of a NWC program and will be reported later.

#### 5.0 SUMMARY AND CONCLUSIONS

The feasibility of using a PSI system to obtain insitu particle size distributions from rocket exhaust propellant has been demonstrated. Measurements have been made of propellant samples fired into a small mixing chamber and in the edge of small solid motor plumes. The PSI data show that the size distributions generated by these devices are strong functions of time indicating the need to be able to sample such distributions rapidly and to obtain the data in large quantities. The PSI measurements show a bimodal size distribution with mode sizes less than 0.5 and at about 3.0 micrometers for a rocket propellant sample measured in the mixing chamber. Comparison of the PSI and commercial optical counter data shows reasonable agreement in the probability density function of sizes less than 0.5 micrometers and greater than 1 micrometer. There is a discrepancy between the measurements and the 0.5 to 1 micrometer range. When the particle data from the PSI and commercial optical

counter is compared with that obtained with multiple wavelength transmissometers there is considerable disagreement. Transmissometer data suggest that either the particle sizes are much smaller or number densities are much higher than detectable with the single particle instruments for the measurable size ranges. The results show that no one particle size instrument can yet give convincing and unquestionable measurements. The PSI data suggests that insitu measurements may vary significantly from instruments which must withdraw a sample from the original environment. Extreme caution must therefore be exercised in interpreting experimental results for theoretical predictions. These measurements have clearly demonstrated that 1) secondary smoke measurements are possible with a PSI system, that 2) number densities are not prohibitively high for this size range and that 3) the rocket plume measurements show that the background light is not significant for points of observation near the plume edge.

REFERENCES

1. MIRADCOM SCF Report-Thorne, L. B. and Wharton, W. W., "Signature Characterization of Propellants ( )," presented at 1976 JANNAF Propulsion Meeting. (CPIA Publication 280, Publication CONFIDENTIAL).
2. W. M. Farmer, K. E. Harwell, J. O. Hornkohl, and F. A. Schwartz, "Calibration of a Particle Sizing Interferometer," Technical Report No. GD-78-1, Contract Number N00174-C-0234, Jan. 1978.
3. See for example, M. Born, and E. Wolf, Principles of Optics, 3rd Revised Edition, Pergamon Press, New York, 1964, pp. 395-398.
4. W. M. Farmer, "Sample Space for Particle Size and Velocity Measuring Interferometers," Applied Optics, 15, 1984 (1976).
5. W. M. Farmer, "Measurement of Particle Size Number Density, and Velocity Using a Laser Interferometer," Applied Optics 11, 2603 (1972).
6. N. A. Fuchs, The Mechanics of Aerosols, Pergamon Press, New York, 1964, pp. 250-257.
7. W. P. Chu and D. M. Robinson, "Scattering From a Moving Spherical Particle by Two Crossed Coherent Plane Waves," Applied Optics, 16, 619, (1977).
8. D. W. Roberds, "Particle Sizing Interferometry," Applied Optics, 16, 1861 (1977).
9. R. J. Adrian and K. L. Orloff, "Laser Anemometer Signals: Their Visibility Characteristics and Application to Particle Sizing," Applied Optics, 16, 677, (1977).
10. D. D. Cooke and M. Kerker, "Response Calculations for Light-Scattering Aerosol Particle Counters," Applied Optics, 14, 734, (1975).
11. E. Miller, "The Dynamics of Secondary Smoke Generation in Smokeless Solid Propellant Plumes," 1975 JANNAF Propulsion Meeting, CPIA Publication 266, Paper Unclassified.

TABLE I

LONG COUNT = 000008  
 SHORT COUNT = 000005  
 PRECOUNT = 000003  
 NUMBER OF READINGS INTO MEMORY = 00300  
 MAX PERIODICITY (%) = 5.000000  
 FRINGE PERIOD = 5.417000  
 HIGH PASS FILTER SETTING (MHZ) = 3.000000E-02

	HISTOGRAM BIN NUMBER																				
	NUMBER OF PARTICLES IN BIN																				
01 00000	02 00000	03 00000	04 00000	05 00001	06 00002	07 00003	08 00004	09 00002	10 00000	11 00001	12 00001	13 00003	14 00001	15 00001	16 00002	17 00000	18 00000	19 00001	20 00001	21 00005	22 00000

MEAN SIGNAL TIME PERIOD (USEC.)  
 NORMALIZED TURBULENT INTENSITY  
 KURTOSIS OF SIGNAL

	NUMBER OF READINGS IN AVERAGE
15.64741	58.86315
1.851390	00230

X-BAR = .6313334  
 SIGMA-X = .2754147  
 COVARIANCE = 1.568486  
 SLOPE = 21.42194  
 Y-BAR = 16.20322  
 SIGMA-Y = 7.946788  
 CORRELATION = .7166413  
 INTERCEPT = 2.592415  
 N = 00030

X-BAR = MEAN VALUE OF D/6  
 Y-BAR = SQUARE ROOT OF MEAN VALUE OF

V (m/sec.)	Visibility	Particle Size (um)	Scatter I <sup>1/2</sup>	Particle Size (um)
.2232715	.9324864	1.245910	11.19740	2.175957
.2262058	.5941392	3.412710	14.62023	3.041495
.2037530	.8971519	1.625100	9.441626	1.731971
.3015495	.6951651	2.871010	10.86345	2.091510

THIS PAGE IS BEST QUALITY PRACTICABLE  
 FROM COPY FURNISHED TO DOD

TABLE II

DISTRIBUTION FUNCTION AND WEIGHTING FACTORS RESULTING  
FROM VARIATIONS IN THE ILLUMINATING FRINGE VISIBILITY

Z AXIS TRAJECTORY POSITION (m)	VISIBILITY FOR A POINT PARTICLE ( $C_1$ )	HISTOGRAM BIN LOCATION FOR CORRESPONDING VISIBILITY	PROBABILITY OF VISIBILITY OCCURRENCE ( $V \leq C_1$ )	PROBABILITY DENSITY ( $V \leq C_1$ )	WEIGHTING FACTOR
0.0	1.0	1	1.0	0.126	1
0.1	0.983	2	0.99	0.126	1
0.2	0.94	5	0.872	0.126	1
0.3	0.871	6	0.746	0.123	0.976
0.4	0.785	9	0.623	0.119	0.944
0.5	0.689	11	0.504	0.113	0.896
0.6	0.591	13	0.391	0.106	0.841
0.7	0.495	15	0.285	0.096	0.76
0.8	0.407	16	0.189	0.084	0.66
0.9	0.326	18	0.105	0.068	0.593
1.0	0.259	19	0.037	0.037	0.293

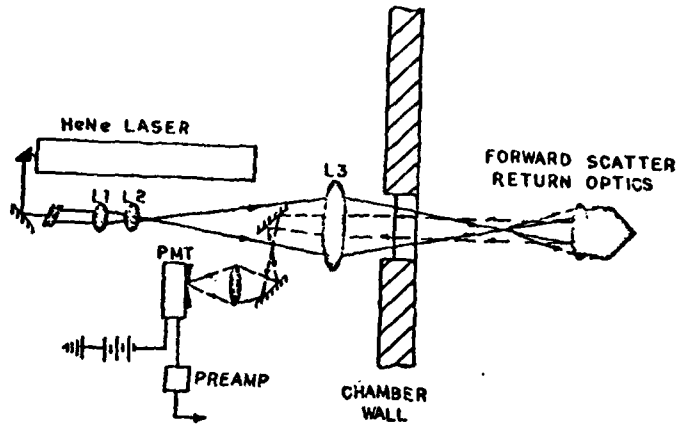


Fig. 1 PSI OPTICAL GEOMETRY FOR MIXING CHAMBER MEASUREMENTS.

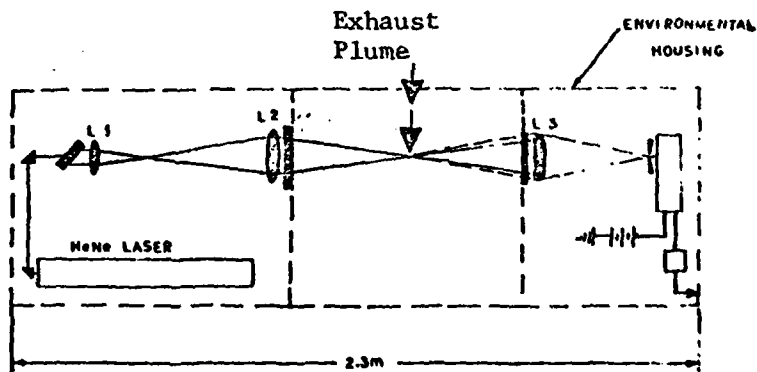


Fig. 2 PSI OPTICAL GEOMETRY FOR ROCKET PLUME MEASUREMENTS

THIS PAGE IS BEST QUALITY PRACTICABLE  
FROM COPY FURNISHED TO DDC

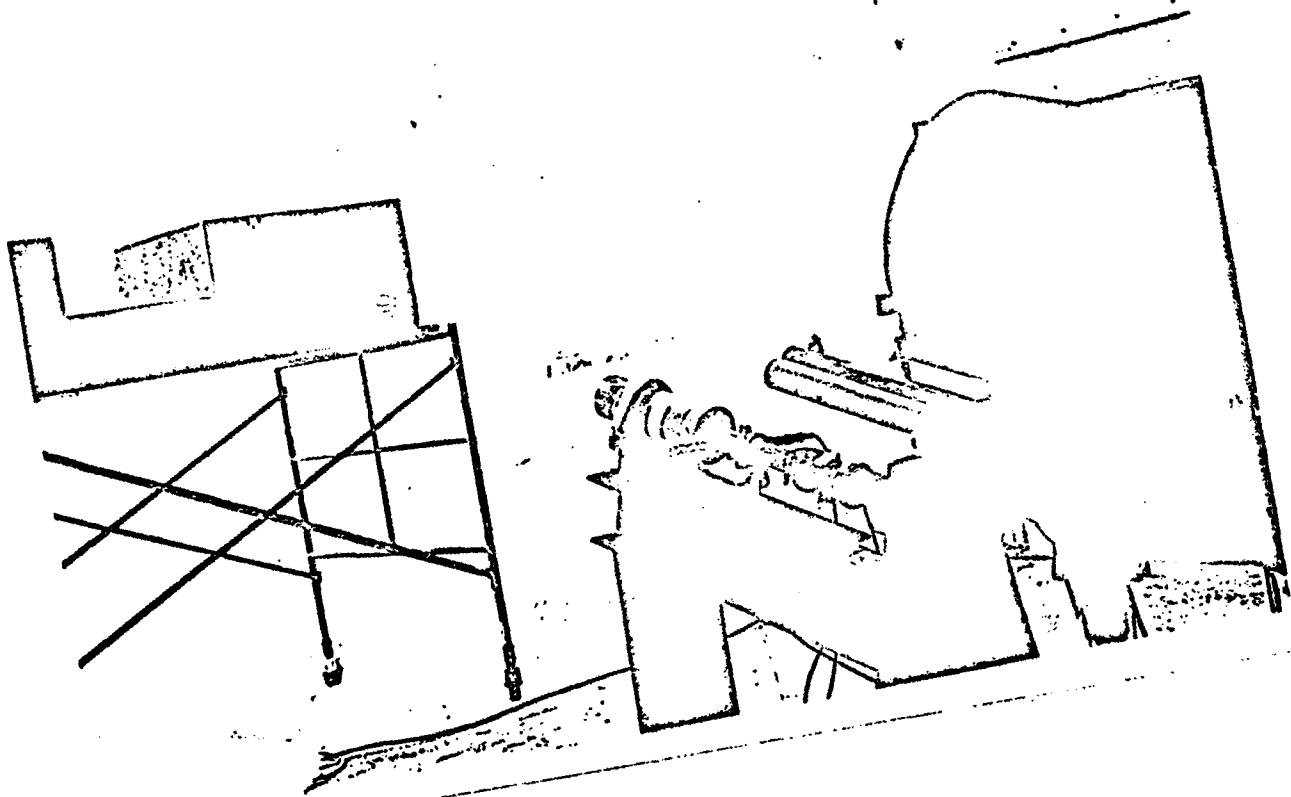
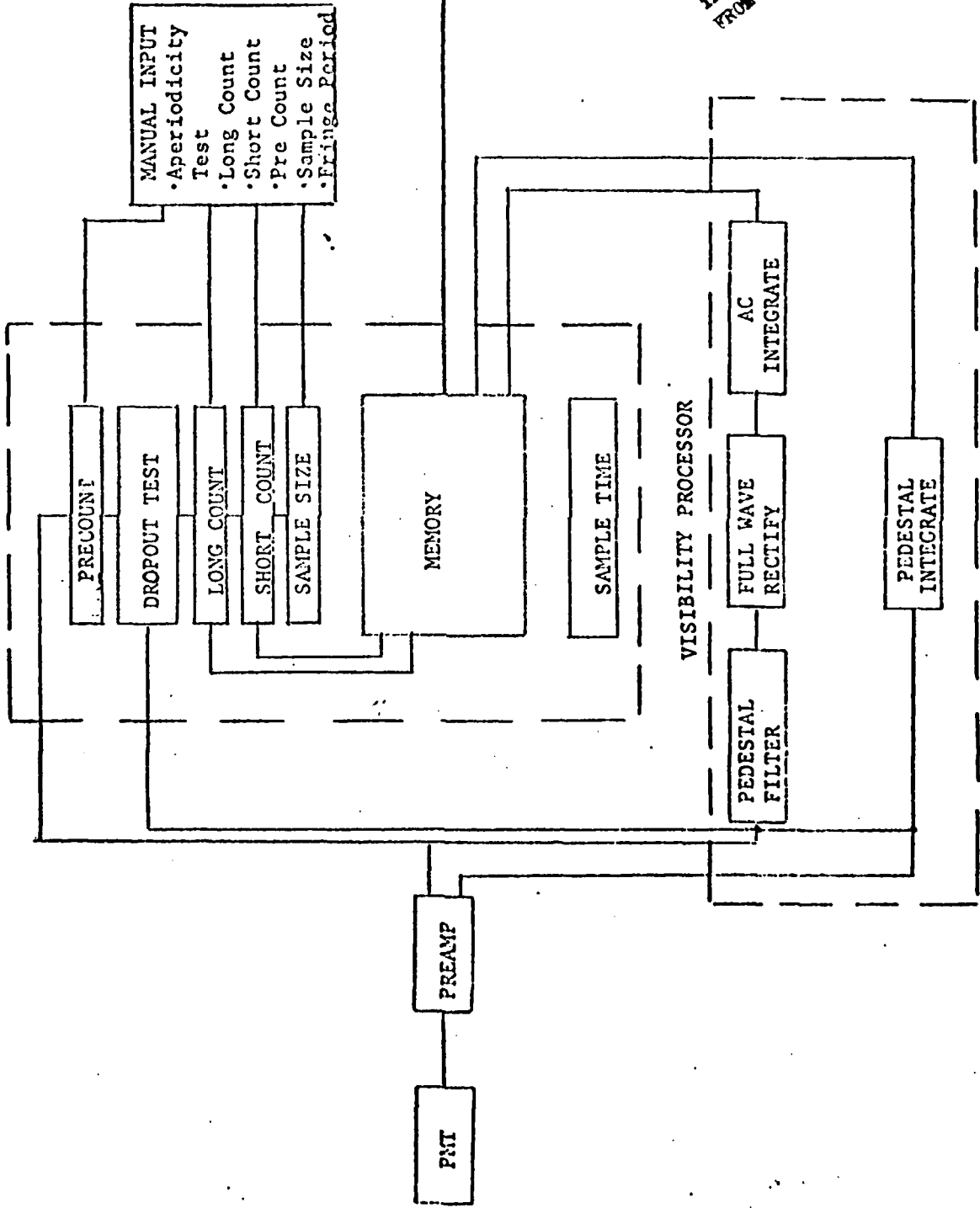


Fig. 3 PHOTOGRAPH OF TEST ARRANGEMENT AT ABL.

S3-PA



DATA OUTPUT

- Particle Size
- Histogram
- Mean Signal Period
- Signal Period
- Scattered Intensity
- Events
- Fraction of Total Population Sampled

THIS PAGE IS BEST QUALITY PRACTICABLE FROM COPY FURNISHED TO DDC

Fig. 4 BLOCK DIAGRAM OF SIGNAL PROCESSING AND DATA MANAGEMENT SYSTEM.

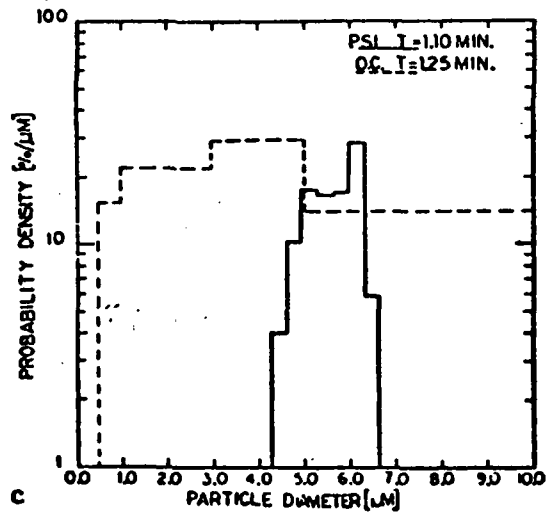
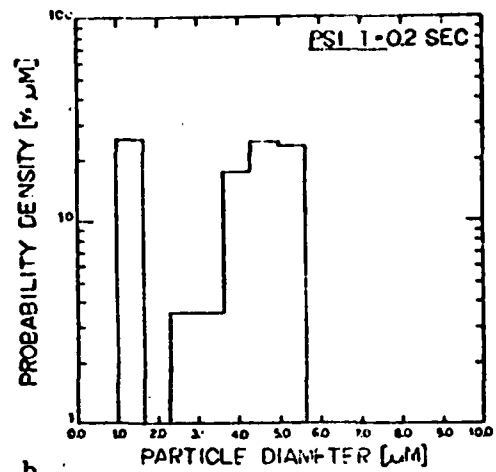
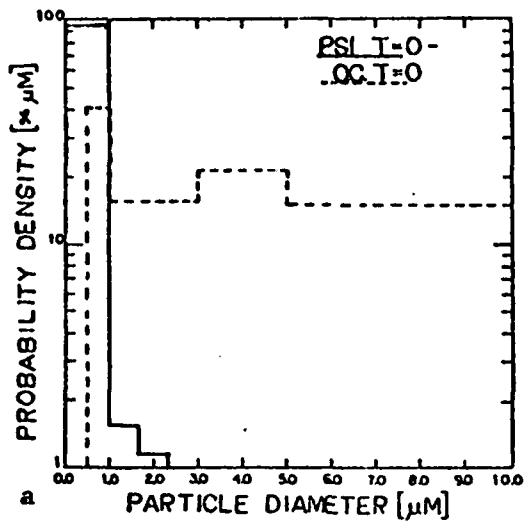


Fig. 5 (a,b,c) Examples of urea-formaldehyde particle size histograms obtained with a PSI and a commercial optical counter.

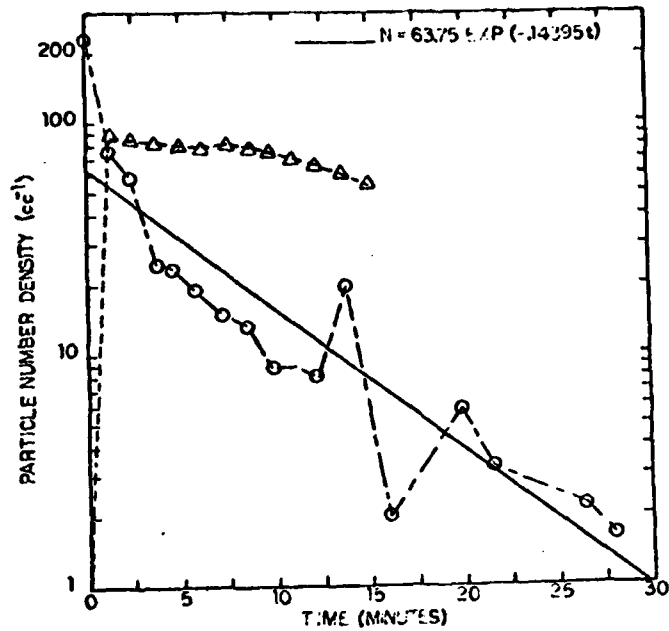


Fig. 6 Urea-formaldehyde particle number density in the mixing chamber as a function of time.

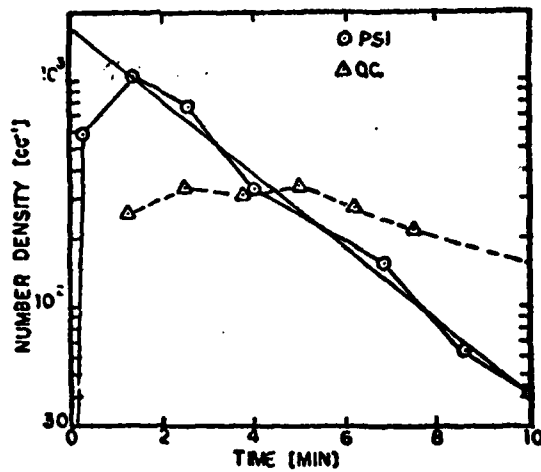


Fig. 7 Particle number density as a function of time in the mixing chamber for a rocket propellant exhaust sample.

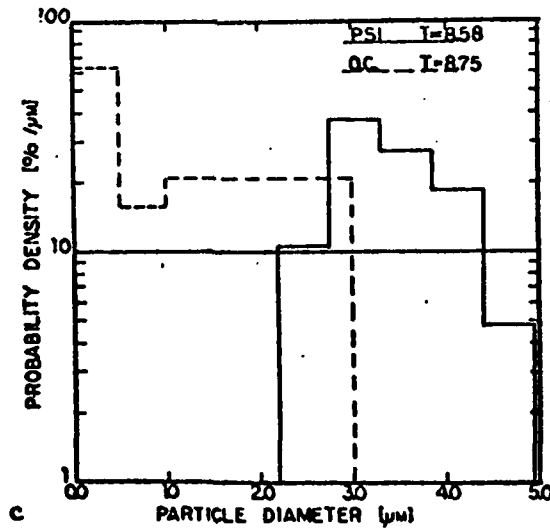
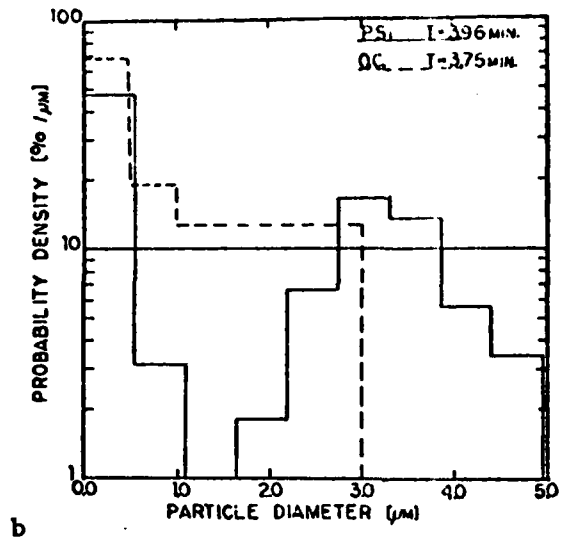
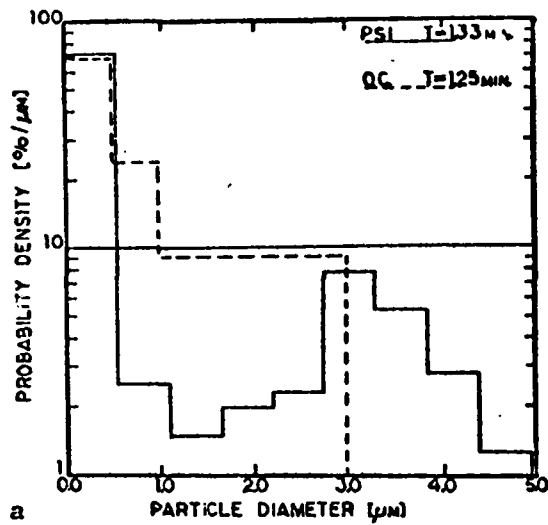


Fig. 8 (a-c) Comparison of rocket exhaust size histograms obtained with a PSI and commercial optical counter in the mixing chamber.

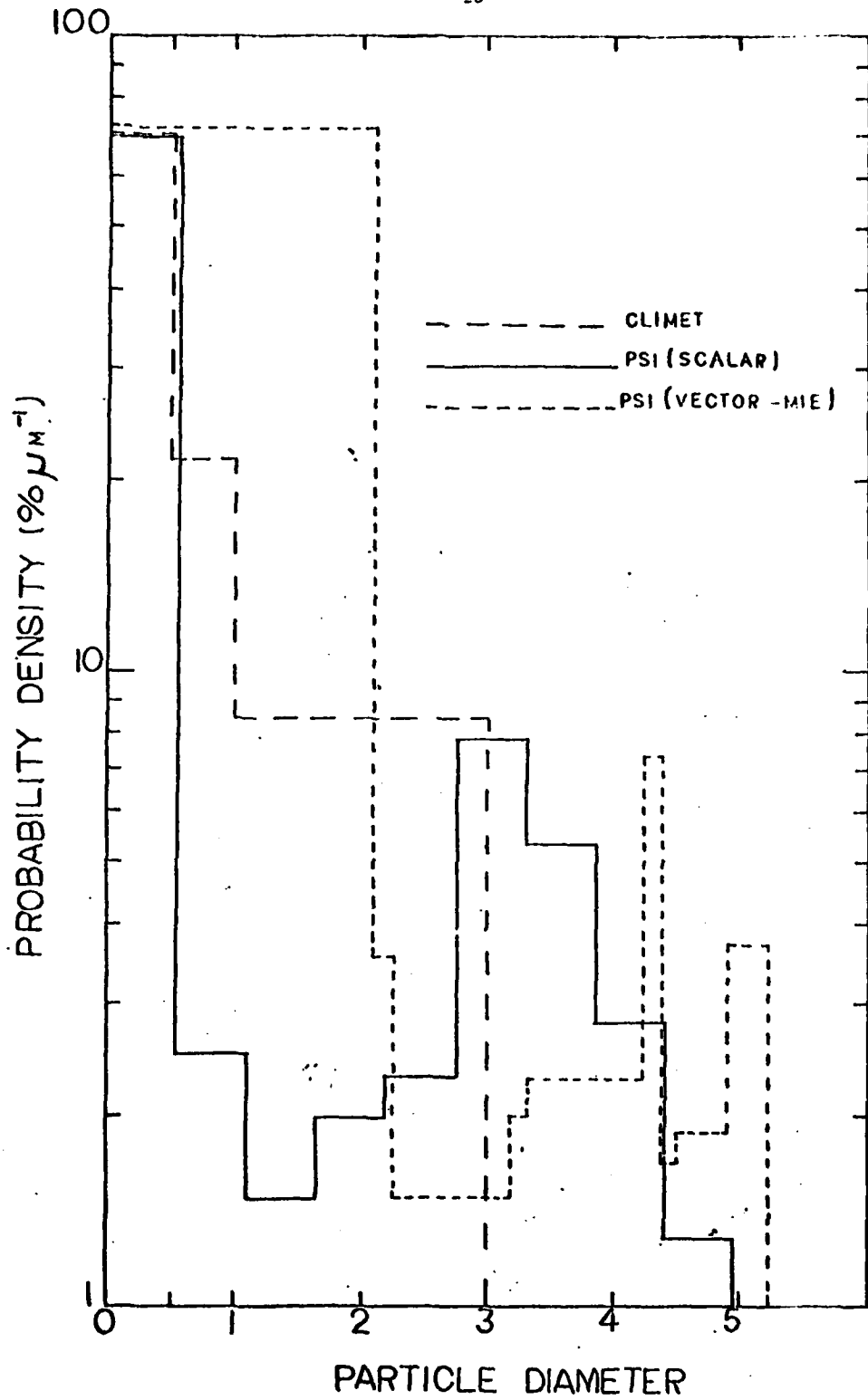


Fig. 9 COMPARISON OF PARTICLE SIZE HISTOGRAMS OBTAINED USING A VISIBILITY FUNCTION DERIVED FROM 1) SCALAR SCATTERING THEORY, 2) MIE SCATTERING THEORY, AND 3) A COMMERCIAL OPTICAL COUNTER.

APPENDIX I

The computer codes used in this project were programmed directly into the microprocessor memory, so that program listings and cards are not available without a great deal of difficulty.

The following material described the UTSI LDV/PSI processor.

## THE UTSI LASER DOPPLER VELOCIMETER AND PARTICLE SIZING INTERFEROMETER SYSTEM

This discussion will describe the primary features of the UTSI Laser Doppler Velocimeter and Particle Sizing Interferometer System which has been developed by the personnel of the Gas Diagnostics Research Division.

### Optical System for UTSI LDV-PSI System

The optical system for the UTSI LDV-PSI systems consists of five primary sub-systems. These are described as follows, and schematically illustrated in Figs. 1 and 2.

The first sub-system is the Bragg Cell Beam Splitter as shown in Fig. 1. The Bragg Cell contains two ultrasonic transducers which operate at 15 and 22.5 MHz respectively. The transducers are housed in a stainless steel housing which is mounted to a tilt adjustment for each of two rotations about axes which are orthogonal and perpendicular to the plane of the optical system. The Bragg Cell housing is stainless steel in order that fluids of different viscosities and acoustic properties can be used to obtain a broad range of beam split angles. The entire Bragg Cell housing can be rotated through  $90^{\circ}$  in order to establish an arbitrary orientation for the velocity measurement coordinate system.

THIS PAGE IS BEST QUALITY PRACTICABLE  
FROM COPY FURNISHED TO DDC



Fig. 1 D<sup>2</sup>BC Beam Splitter

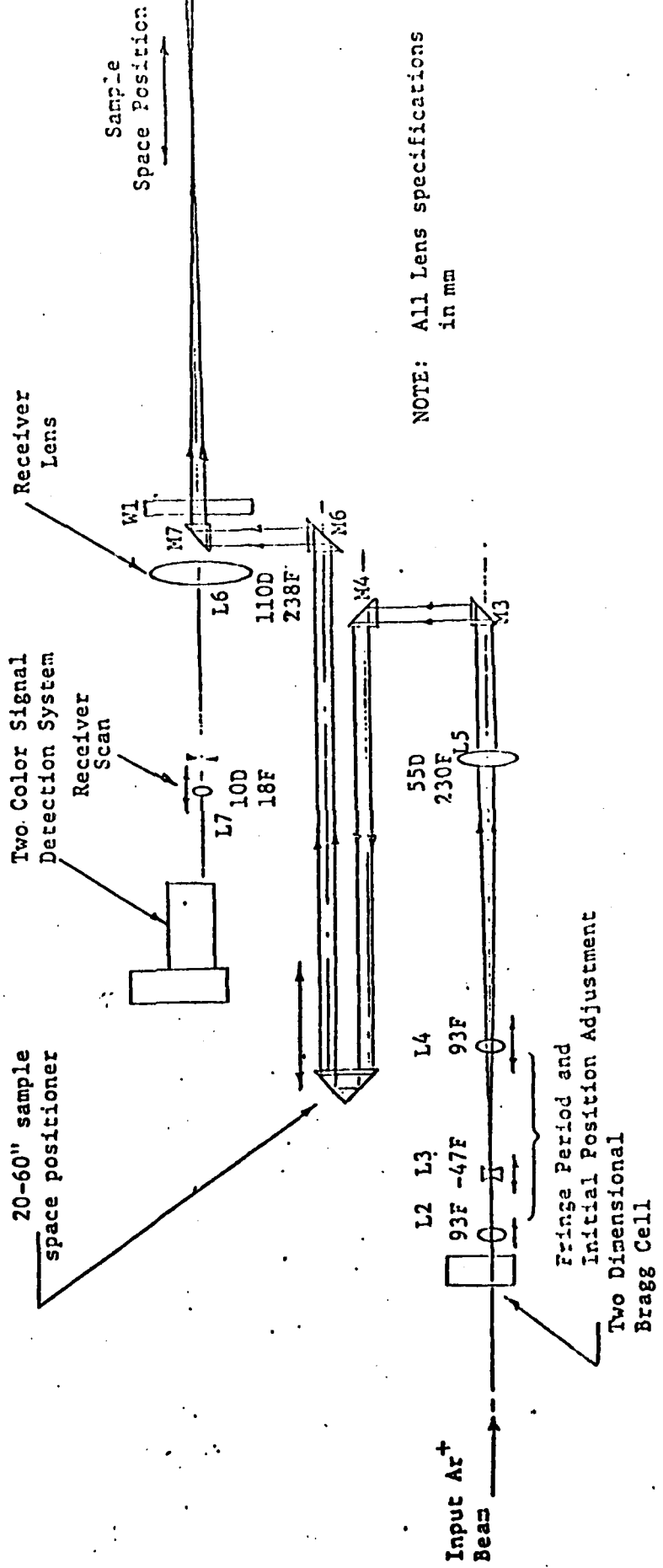


Figure 2. Schematic of the Optical System for the UTSI Particle Morphokinometer

The second sub-system consists of lenses L2 through L5 (see Fig. 2). These lenses control the value of the fringe period in the sample space and the maximum focus position for the optical system. By suitably adjusting these lenses, a fringe period ranging between 70 and 377 microns for the 15 MHz channel on the Bragg Cell and between 47 and 251 microns for the 22.5 MHz channel on the Bragg Cell is possible for various focus positions ranging between 0.5 and 1.5 meters. The primary function of lens L2 is to control the beam diameter and hence the number of cycles present in the sample space in the instrument. Lenses L3 and L4 are used primarily to control the focus position and fringe period of the sample space. Lens L5 represents the primary transmitting lens.

The third major sub-system of the optical system consists of the scanner for the transmitter portion of the optical system. The scanner consists of a set of mirror prisms which fold the optical path along a screw drive positioner. The screw drive positioner is such that it can move a total of 20". Since the beam path is folded along the screw drive, a traverse distance of 20" along the screw drive corresponds to a sample space scan variation of approximately 40". The position of the reflecting prism mounted on the screw drive is read with a potentiometer bridge to an accuracy of  $\pm 0.005$ ". The position of the sample space has been correlated with the screw position such that the readout on the scanner control panel is read directly in inches.

The fourth primary sub-system of the optical system consists of the 10 cm receiver lens and the focus scan system. The focus scan

system is designed such that a collimating lens and limiting aperture can be positioned at the image of the geometric center of the sample space in order to collimate the input to the detection system. A closed loop servo-system controlled by a microprocessor will allow the transmitter and receiver to continuously scan. The limiting aperture consists of a variable iris for typical operation. However, if increased spacial resolution is required, a number of fixed apertures can be inserted into the rear of the iris.

The fifth primary sub-system consists of the dual color light detection system. The optical system has been designed such that full power utilization of the laser can be obtained by using this light detection system which consists of a color separator that separates the light scattered from both primary colors produced by the laser (514.5 and 488 nm). After the colors are separated they are passed into a set of 10 Å bandpass interference filters which pass the scattered laser light but remove a large portion of the background radiance. The light is then brought to a focus on the photocathode of the photomultiplier tube being used to convert the scattered light into an electrical signal. A viewing system is provided in the light detection system in order that the operator determine optimum system focus characteristics and that the return from both beam colors is suitably imaged onto the photomultiplier photocathode.

#### Photodetector System

The photomultiplier tube used for detecting the light signal is an EMI Model 9781R tube. The typical quantum efficiency for

-33-

this tube at 514.5 nm is approximately 12% and 488 nm is approximately 13%. Typical gain for the tube is  $5 \times 10^5$ . The photomultiplier tube gain which is voltage controlled is a significant parameter in limiting the depth of field and particle size range which can be detected with the optical system. The photomultiplier tube output will enter a pre-amplifier which will be attached to the optics shelf. The function of the preamplifier is to increase the absolute output of the photomultiplier tube signal to a level which is acceptable by the signal processor.

Signal Processor (see attached Specifications for LV Processor)

The signal processor processes the photomultiplier signal to obtain two parametric measurements---velocity and particle size. The velocity will be determined by measuring the scattered light signal time period. The direction of the velocity vector will be determined by the absolute magnitude of the signal frequency relative to a reference frequency and the particle size will be determined by measuring the signal shape. The velocity components and direction will be identified using signal separator and conditioning electronics. The function of these electronics will be to condition the signal from the PMT. It will filter the sum and difference carrier frequencies which are present in the scattered light signal. It then separates the signals corresponding to the 15 and 22.5 MHz channels (or higher carrier frequencies as necessary). Thirdly, it introduces a switch selectable carrier (or difference) frequency which can vary from 0 to 990 KHz in the low range in 10 KHz steps or 100 KHz to 10 MHz in 100 KHz steps in the high range. The function of this carrier

frequency is to optimize signal-to-noise ratio and to introduce high accuracy into the frequency measurements. The signal conditioner will also contain a low pass filter which rejects the sum and difference components introduced into the heterodyne process when the carrier frequency is selected. After the velocity component signals leave the signal conditioner, the signals will enter the signal processors where the signal time period is determined by measuring the signal for two different period averages. The number of cycles in each average will be a pre-determined system constant which is programmable from 0-256 in unit increments. These averages are used in aperiodicity tests to determine that the signal is of acceptable quality before it is recorded by a data acquisition system. Particle size measurements are accomplished by measuring the signal visibility. In addition, the mean value of the scattered light signal will also be measured such that when the mean value and the signal time period are calculated, the scattered intensity can also be measured and the particle size estimated from Mie scatter theory. The signal processors will have built-in time period calibrators which are front panel accessible.

#### Data Sorter

The signal processing system is equipped with a small data acquisition system. This device will be used to acquire large amounts of a data in a histogram format. It is equipped with programs which allow the recording of various system parameters in addition to measured data. The data which can be acquired with this system includes velocity histograms covering four decades of velocity variation, particle

size histograms which are programmed in terms of the signal visibility measurements and correlated directly with a library function which relates signal visibility to particle size. Also, included in these programs are weighting factors which allow the normalization of the histogram such that equal sample space volumes are compared for the particle number density measurements. It will indicate the number of "events" or attempted measurements by the signal processor and it will record the total data acquisition time, or the acquisition time for each measurement.

## SPECIFICATIONS FOR LV PROCESSOR

Signal Input Frequency Range - Maximum Frequency = 100 MHz  
Minimum Frequency given by

$$F(\text{min}) = \frac{| F_c (N_L + N_P + 1) |}{2^{20} - 1}$$

$N_L$  - Long Fringe Count

$N_P$  - Precount

$F_c$  - Clock Frequency (500 MHz)

$F(\text{min}) \approx 5$  kHz for  $N_L = 8$ ,  $N_P = 1$

Signal Input Amplitude - 300 Microvolts to 3 volts RMS for frequency less than 50 MHz.

Count Sequences - The long fringe count,  $N_L$ , is programmable from 2 to 255. The short fringe count,  $N_S$ , is programmable from 1 to 254. The precount,  $N_P$ , is programmable from 1 to 15.

Dead Time - Time to store a reading including the hardware clock reading = 3.7 microseconds (=2.5 microseconds if hardware clock is not read).

Recovery Time from Signal Dropout - Depends upon when dropout occurred. Recovery time,  $T_R$ , is approximated from

$$T_R = N_D T_D / 2$$

$N_D$  - Number of fringes counted before dropout.

$T_D$  - Signal Frequency

Recovery Time from Noise Spike - Time required for recovery from a single noise spike which starts fringe counters, 0.5 microseconds

Doppler Period Resolution - Value of the least count in the measured Doppler period for the highest Doppler frequency. Depends upon the setting of the long fringe counter.

$$\begin{aligned}\Delta T &= \frac{1}{N_L f_c} \\ &= 10 \text{ picoseconds for } N_L = 255 \\ &= 250 \text{ picoseconds for } N_L = 8\end{aligned}$$

Hardware Clock - Records time at which each reading is taken. Clock resolution is 1 to 200 microseconds in 1,2,5,10 steps.

Aperiodicity Limit - Aperiodicity error, E, is computed from

$$E = 100 \times \frac{N_L - \frac{N_L}{N_S} N_S}{N_L}$$

where  $N_L$  is the number of counts acquired in a counter which counts clock pulses ( $f_c = 500 \text{ MHz}$ ) for a time duration  $N_L T_D$ . Similarly  $N_S$  is the number of counts acquired in a time  $N_S T_D$ . The operator may choose any value for  $E_{\text{max}}$ . The processor will compare this with  $N_S$  to insure that the chosen E (expressed as a percentage) is consistent with the available resolution (i.e.,  $100/E_{\text{max}}$  must not exceed  $N_S$ ).

Controls - All functions, except power on and reset, are controlled by a 25-key keyboard.

Display - 16-digit having full ASCII character set.

Outputs - A 16-bit 3-state bidirectional data bus provides interface capability to virtually any digital device. Decoding is provided for up to 8 devices on the bus. An RS/232 interface having variable baud rates is also provided.